Low Inductance Effects on Electric Drives using Slotless Permanent Magnet Motors: a Framework for Performance Analysis

Matteo Leandro, Nicola Bianchi
Department of Electrical Engineering
University of Padova
Padova, Italy

Marta Molinas
Department of Engineering Cybernetics
NTNU
Trondheim, Norway

Ravindra Babu Ummaneni
Alva Motor Solutions
Trondheim, Norway

***Abstract*—The use of slotless Permanent Magnet machines is becoming the first choice among many other conventional solutions when improved features, such as smooth control and very high speed, are needed. However, it is not often mentioned that in order to take advantage of the main peculiarities of this kind of machines, the whole electric drive system should be conveniently designed to avoid an unexpected decline in performance during the operation. Whenever the behavior of a motor needs to be studied by means of Finite Element Analysis (FEA) as a verification of a design process, the under-load condition is typically simulated by assuming ideal current waveforms as coil sources i.e. sinusoidal for Synchronous machines and quasi-squared for Brush-less DC (BLDC) machines. However the characteristic low inductance of slotless machine can lead to high current ripple and hence, torque ripple, if the supply system is not consequently designed. This work aims to define a framework capable of giving some useful information regarding the electric drive performance. Such a framework is based on a model representing the electric drive system which gives, indirectly, the supply current to a Finite Element (FE) motor model, in order to carry out a harmonic losses analysis based on a temporal discretization technique. A slotless motor prototype has been considered as an example and different solutions for the current ripple reduction are also discussed.**

***Index Terms*—slotless machines, electric drives, time-stepping FEA, harmonic losses, motor controllers, power inverter, drive modelling**

I. Introduction

Slotted electric machines are nowadays leading the wide market of electric machines starting from large machines for power generation, down to small hand-tools motors for everyday use. Brushless Permanent Magnet (PM) solutions are particularly attractive when high speed operations are required. In these operating conditions particular solutions should be adopted to ensure high efficiency operation in the whole speed range. Slotless machines are playing a crucial role in this regard, ensuring considerable high-speed losses reduction, because of the absence of the slot-opening effects on the air-gap flux density distribution. The latter is the main cause of eddy-current losses in PM slotted machines as widely discussed in [1] where the effect of space harmonics in the magnetomotive force (MMF) is also considered, in [2] the dependency on main machine design parameters is investigated as well. It is worth to notice that these losses could lead to high temperature in the magnets themselves, increasing the risk of demagnetization. In so far as none of the effects related to the slot existence comes into picture for PM slotless machines, one could think that magnets losses should not be a problem to consider, at all. The latter statement would hold, if ideal (sinusoidal) source currents were considered; however, the use of inappropriate control techniques of the motor itself (such as: low switching frequency at the power inverter and or trapezoidal control) can lead to a significant breakdown in the motor performance.

The geometry of the motor used in this case study, is depicted in Fig. 1 where a two-pole section is considered to speed up the Finite Element Analysis (FEA). The rotor is made up of two concentric back-iron parts, separated by an air-gap. A Halbach-array is attached to the inner surface of the outer back-iron (out-runner motor). The stator consists of a three-phase winding enclosed in epoxy resin, which is located in between the magnets and the inner back-iron. This gives to the geometry a "double-airgap" configuration. The inner back-iron is part of the rotor assembly, and thus, it is a rotating part. It can be noted that the magnetic airgap spans radially from the outer surface of the inner back-iron to the inner surface of outer back-iron; this means that the stator windings are working in a magnetic circuit which exhibits higher reluctance with respect to slotted motors and hence, the winding inductance can be much lower. In [3] a hypothetical range of definition for the inductance in slotless machines is given as a factor, with respect to conventional machines as 1/10 to 1/100 of the latter ones; however the inductance itself is dependent on many design parameters which needs to be considered when making this kind of comparisons (e.g. airgap thickness, number of turns which are, in some sense, related to each other since the increase in the number of turns could lead to the increase in the stator thickness, and hence, the airgap itself) .

The chopped voltage generated by a power inverter is the cause of ripple in the motor current; moreover, the lower the switching frequency and the motor inductance the higher the current ripple. The current variation with respect to the

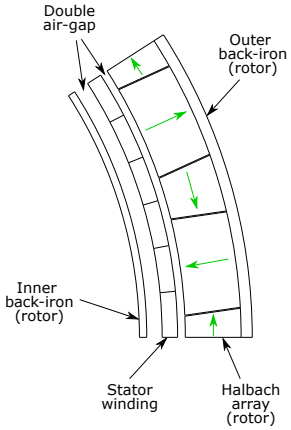

Fig. 1. Two-poles section of the tested prototype

ideal sinusoidal waveform generates harmonic fields in the motor, and this leads to torque ripple, high harmonic losses (iron losses, magnet losses, conduction losses) and audible noise, if consistent harmonics appear below 20 kHz. This work introduces a losses analysis based on time-stepping (temporal discretization) technique by means of an automatic code coupled with a Finite Element Method Magnetics (FEMM) model of the motor [10]; the code receives as an input (source of the FE coil representation) the resulting current waveform from the electric drive model, where a Space Vector Modulation (SVM) is implemented for the inverter control algorithm. The model is controlled by a main script where all the useful parameters are loaded and a convenient design of the Proportional Integral (PI) controller for both the speed loop and the current loop is implemented. The idea behind this type of implementation is based on the so-called circuit coupled Finite Element Analysis (FEA) implemented in some commercial software. However, in those cases one typically tries to take fully advantage of the FEA transient solver and get all the information out of the solver itself to minimize the post-processing; this requirement is usually translated in long computational times; in [5] a thorough analysis of electric drive losses is performed by means of this method, but already at 37 kHz switching frequency some 80 hours were required to carry out the whole analysis. The method suggested in this work is meant to be the first iteration of a potential alternative solution to the aforementioned one, and to all those problems in which trying to find an analytical solution of the problem is anything but easy.

II. Electric Drive Model

The electric drive system implementation has followed three fundamental steps:

- SVM algorithm implementation in a dedicated routine;
- State space model implementation of the electric motor, based on the electrical and mechanical equations;
- Code implementation for the PI controller design, based on the Bode plot analysis of the system transfer function.

The drive system is based on the control of the two components vector, resulting from the dq-Park transformation of the electrical quantities (currents), in a reference frame which is rotating synchronously with the "electrical coordinate" of the rotor; let ϑ_m be the mechanical angular coordinate of the rotor, then:

$$\vartheta_{me} = p\vartheta_m \tag{1}$$

where p is the number of pole pairs and ϑ_{me} the electrical coordinate

A. SVM Implementation

The three-phase power inverter is implemented as a function which handles a set of inputs from both model input parameters (DC supply voltage, switching frequency) and output parameters (reference vector voltage from current controllers, simulation time), to give as an output the voltages applied to the motor terminals. The SVM implemented in such a code is analogous to a PWM control with triangular third harmonic injection in the sinusoidal modulation signal, as described in [3], but the implementation which has been adopted, considers the position of the reference vector voltage and evaluates, as a consequence, which switches to control and the relative timing to represent that very voltage [4]. The motor line to line voltages are then computed out of the inverter output voltages and given as an input to the motor state space model.

B. Mathemeatical Model of the Electric Motor

The model of the electric motor is implemented considering the stator electrical equations:

$$v_x = Ri_x + L\frac{di_x}{dt} + e_x \tag{2}$$

with: $x = a, b, c$ phase index, R motor phase resistance, L synchronous inductance, i_x phase current, e_x induced back-electromotive force (back-emf) and v_x phase voltage.
The phase voltage equations shown in (2) can be conveniently rearranged in order to get the expression for the two line to line voltages:

$$\begin{aligned} v_{ab} &= v_a - v_b = R(i_a - i_b) + L\frac{d(i_a - i_b)}{dt} + (e_a - e_b) \\ v_{bc} &= v_b - v_c = R(i_b - i_c) + L\frac{d(i_b - i_c)}{dt} + (e_b - ec) \end{aligned} \tag{3}$$

By combining the two latter voltage equations, the two following differential equations for the two phase currents i_a, i_b can be written:

$$\begin{aligned} \frac{di_a}{dt} &= -\frac{R}{L}i_a + \frac{2}{3L}(v_{ab} - e_{ab}) + \frac{1}{3L}(v_{bc} - e_{bc}) \\ \frac{di_b}{dt} &= -\frac{R}{L}i_b - \frac{1}{3L}(v_{ab} - e_{ab}) + \frac{1}{3L}(v_{bc} - e_{bc}) \end{aligned} \tag{4}$$

The back-emf is computed internally in the model assuming a sinusoidal variation with respect to the electrical coordinate. Though, any other kind of waveform could be set e.g.

trapezoidal to simulate a BLDC control algorithm. From the solution of the two equations in (4), the third current can then be computed by enforcing $i_a + i_b + i_c = 0$.
The electromagnetic torque Te can be expressed as it follows:

$$T_e = \frac{(i_a e_a + i_b e_b + i_c e_c)}{\omega_m} \tag{5}$$

and the resulting torque is then used to get the mechanical angular speed ω_m from the torque balance equation at the motor shaft:

$$T_e = B\omega_m + J\frac{d\omega_m}{dt} \tag{6}$$

where B is the friction coefficient and J the moment of inertia. Finally, (4),(5) and (6) are plugged into the same state space system representing the electric motor, which gives phase currents, rotational speed and angular mechanical position from the latter, as an output.

C. PI Controller Design

The model is provided with three different PI controllers: two current controllers (one for each of the two current vector components in the dq reference frame) and a speed controller. The control of the drive follows a Maximum Torque Per Ampere (MTPA) approach and since the motor under consideration has no reluctance effect, this is done by keeping the reference for the q-current to zero i.e. current in phase with the back-emf. The design of the controllers has been carried out by considering the transfer-function based system i.e. each component of the system has been represented with the equivalent transfer function. The frequency response of the system has then been analyzed in order to tune both the proportional and the integral gains so that the response of the system to a step variation (either in the speed reference or in the current reference) was fast (low rise time) and stable (without overshoots) at the same time; this is done indirectly by setting a requirement in the frequency domain to the system Band-Width (BW) and Phase-Margin (PhM). An automatic code accomplishes to this purpose by building the transfer-function based system from all the input parameters needed (motor parameters, switching frequency of the inverter); the analysis of the Bode plot of the open loop system defines the limit requirement for BW and PhM, such that the closed loop step response is the fastest and either with a limited or without overshoots.

It is worth noting that this fairly easy way of designing the PI controllers, is due to the representation in the dq rotating reference frame of the whole system, which ensures that, ideally, the quantities to be controlled are constant references; these PI controllers, as such, could not attain a good tracking of variable signals [6]. As a matter of fact, the introduction of the inverter switching behaviour in the drive system makes these PI controllers working with references that are anything but constant. If the current feedback is sent back to the controllers as such, the model gives a noise as an output that has nothing to do with the implemented SVM. To solve this problem the currents need to be conveniently filtered before being sent as a feedback(a first order low pass filter, tuned to work at the switching frequency, was shown to be enough). It could be noted that this kind of filter would tend to approximate even better a real application, where the sensor for the feedback cannot be considered ideal in terms of bandwidth, and the sampling time of the feedback can be even lower than the switching frequency.

III. Tested Drive System

The motor geometry is shown in Fig. 1 where a two-pole section is represented in FEMM to speed up the loss analysis. The rotor is made up of two concentric back-iron parts separated by an air-gap. A Halbach-array is attached to the inner surface of the outer back-iron (out-runner motor). The stator consists of a three-phase winding enclosed in epoxy resin, which is located in between the magnets and the inner back-iron. This gives to the geometry a "double-airgap" configuration. The inner rotating back-iron is a design choice to increase the available torque, and since it is rotating synchronously with the magnetic field there is no need for laminations.
The windings are made up of Litz wires, and hence, the AC losses due to skin effect are drastically reduced; however, proximity effect should be considered also depending on the packing factor [8]. For this work all the useful parameters were measured from the prototype itself; however one could take advantage of the take all the parameters needed from either a FEA or analytical models, if existing. Table I shows all the useful parameters to run the drive model; it is worth to notice that the phase inductance assumes a very low value, for this reason the "Connections inductance" is added, in order to account for the current connections to the measurement equipment during the testing phase. Therefore the phase inductance in the model is increased to the sum between L and L_{con}. It is worth to point out the fact that the additional inductors for this prototype appears to be overrated in terms of inductance value.

Nevertheless, the aim of this work was to highlight the effects of having high current harmonics, and hence, the case with these additional inductors offers a best case scenario (as it will be shown). Furthermore, these kind of inductors are designed to operate at quite high frequencies with good performance, because of both the type of material typically adopted (ferrite) and the gapped topology (Fig. 2) which ensures a low flux density operation, especially with the low currents inherent for this case study. The latter comment, along with the low resistance value have led to neglecting the inductors impact on the overall efficiency.

Finally it is worth to mention the other possible solution for the current ripple reduction i.e. having higher switching frequency. The prototype was tested with a conventional motor controller capable of up to 25 kHz switching frequency; however, motor controllers manufacturers are offering interesting solutions [9] using novel technologies in the semiconductor field (Wide band-gap semiconductors), along with optimized

Fig. 2. Additional inductors

PCB design and device topology to ensure fast switching with low EMI issues related to parasitic embedded elements.

TABLE I
MOTOR DRIVE MAIN PARAMETERS

	Parameter	Value	Unit
p	Pole pairs	11	-
R	Phase resistance	0.209	Ω
L	Phase inductance	5.75	μH
Λ_{mg}	Magnets flux	2.17	mVs
I_{lim}	Maximum permissible current (peak value)	8.8	A
U_{lim}	Maximum available voltage (peak value)	60	V
J	Rotor inertia	1.08	$kg \cdot cm^2$
B	Bearign friction coefficient	4	$\mu Nm \cdot s$
f_{sw}	Switching frequency	25	kHz
L_{con}	Connections inductance (per phase)	2	μH
L_{choke}	Choke inductance value	210	μH

IV. FEA Loss Analysis

The method described in [10] was the starting frame for the loss analysis algorithm which has been used for this work. The method is based on the analysis of magnetic quantities (magnetic potential and magnetic flux density) in specific regions of the domain (magnets and iron) , while the stator current is varied according to the rotor position. The source current for this code is the output current from the model solution; it is worth to mention that the variation in the rotor position must be small enough to catch the current variation due to the switching frequency. The method appears to be even more effective when using the air-gap boundary condition; indeed, as described in [11], this ensure that, while the rotor is rotating, the mesh remains the same.
Starting from the solution of the electric drive model (current waveform in steady state conditions), and the motor finite element model, the loss analysis code is built according to three main steps:

1) Post-processing of the current waveform to be used as a source for the FEA;
2) Solution of a "convenient" number of magneto-static problems to build a time varying solution;
3) Post-processing of the FEA results for the losses estimation.

A. Post-processing of Drive Model Results

This step is performed by keeping in mind that a q-axis current needs to be set as a source for the FEA model, in order to achieve the same MTPA operation as the drive model simulates. With this in mind, the current waveform is conveniently resampled with a fixed time step, which is set short enough to keep all the information of the current waveform itself; in this regard, it is worth noting that the FEA will be performed for each and every the current samples, and hence, the longer the sampling time, the faster the loss analysis. A Fourier analysis of the resampled waveform, allows to find the fundamental of the signal (phase and magnitude) and therefore, the three-phase current waveform is built by copying and shifting the resampled signal in order to get the equivalent current, in the dq reference frame, oriented along the q-axis. Moreover, the Fourier analysis of the signal allows to define the RMS value of the current waveform (to be used for the conduction loss)

B. FEA

The part of the code controlling the FEA, takes care of setting the correct current sample in each slot and the correct rotor angle depending on the current sample to be considered, or vice versa.
A quite dense mesh is required to get more accurate results out of the loss analysis. In particular, along the two airgaps the maximum angle spanned by a mesh element was set to be ten times higher than the step angle between two simulations as in [11].
At any rotor position the flux densities in all those elements belonging to iron regions are stored in a matrix, and the same is done with the magnetic vector potential for those elements belonging to magnets regions.

C. Post-processing of FEA results

At this point the aim is to perform the Fourier analysis of the stored quantities from the FEA in order to treat each one of the different harmonics as an individual one in terms of losses, and finally all the different contributions are summed-up to find the total losses. Magnets loss and iron losses are computed in the same fashion as in [10].
It is worth noting that in the real prototype the iron parts are not laminated, and therefore, the hypothesis of neglecting any sort of effect on the field distribution because of the iron losses appears to be even more forced in this case study. Moreover the iron losses taken from [10] as such, do not account for minor loops effects on the hysteresis losses [12]. In [13] a method to account for the effect of these minor loops was proposed; however, it was not applicable in this case study, being the loss data for the iron used in the prototype not given.
The iron loss data in terms of hysteresis (C_h), and eddy currents loss (C_e) coefficients (here considered as loss per

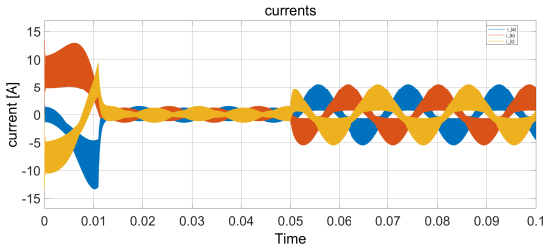

Fig. 3. Current waveforms -dynamic drive response- (torque=0.1 Nm; speed=300 rpm steady state condition)

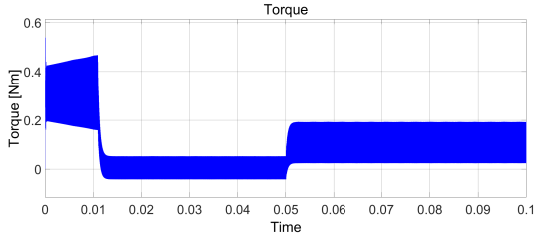

Fig. 4. Torque profile -dynamic drive response-(torque=0.1 Nm; speed=300 rpm steady state condition)

volume) were extrapolated from the M330-50A laminations data-sheet (as reported in [10]), leading to:

$$C_e = 1.183 \left[\frac{W}{m^3 T^2 Hz^2} \right]$$
$$C_h = 137.98 \left[\frac{W}{m^3 T^2 Hz} \right] \quad (7)$$

Finally, the efficiency is estimated considering the losses that the code was called to compute.

V. Simulation Results

Once all the parameters needed to define the electric drive system are known (either from measurements or estimations); the related model based on (4)-(6) As a first simulation the reference speed was set to 300 rpm as a step variation and during the steady-state operation, a load torque is applied in order to reach a reference of 0.1 Nm. In Fig. 3 the current waveforms from the dynamic simulation are shown, Fig. 4 illustrates the resulting electromagnetic torque. In the first stage of the simulation, the control chain keeps the reference torque to the maximum value (0.3 Nm) to reach the reference speed; after about 0.035 s the system reaches the reference speed and thus, the torque/current reference becomes the one needed to balance the friction torque; finally, the step variation in the load torque is applied at 0.05 s and hence, the torque/current reference increases as a consequence. It this case study the rotational speed variations due to the current ripple are negligible because of the relatively high rotor inertia.

The aim was to validate experimentally the results given by the model and the loss analysis; the results shown previously in terms of current waveform will be compared with a current visualization at the oscilloscope. For the loss analysis the aim

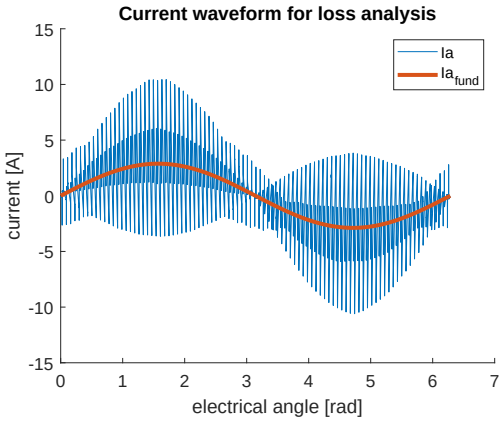

Fig. 5. Output current from the drive model used for the FE analysis -

was to perform it in a certain range of speeds; even though a rigorous approach would have required the analysis to be performed with the resulting current waveform from the drive model simulation for that very speed.

However, it has been shown that the use of a current waveform resulting for a given speed at the drive model, for the loss analysis in a certain speed range, gives fairly good results at lower speeds and at higher speeds as well. This was proved by making three simulations with three current waveforms resulting from three different speed values. It was shown that the speed in the middle gives a slight underestimation of the efficiency at low speed and a slight overestimation at higher speed (in both cases limited to about 2% maximum difference in efficiency). This can be explained considering that in the lower speed case the harmonics amplitude is overestimated, whereas for the higher speed case the harmonics amplitude are underestimated (this is due to the back-emf effect on the current ripple); in any case the current harmonics are located at multiple of the switching frequency, and hence, the harmonic field is always rotating at the same speed. This means that (with respect to the fundamental) in the lower speed case the harmonics would be of higher order, on the contrary, for the higher speed case they would be of lower order. For this reason the current waveform resulting from a speed reference of 1500 rpm was used for the efficiency estimation in the speed range of the experimental measurement (from 0 to 2400 rpm). The sample of the current waveform used in the FEA simulation is shown in Fig. 5, where the switching effect to follow the reference current (fundamental) is due to the low inductance value, combined with the not enough high switching frequency .

The variable speed loss analysis led to the results depicted in Fig. 6.

The same analysis was carried out with sinusoidal current waveform as a source of the FE model (proved that the resulting current with additional inductors gives the same results); the variable speed losses are negligible if compared to the conduction ones which remain constant for the whole range (being the current fixed). The efficiency comparison with

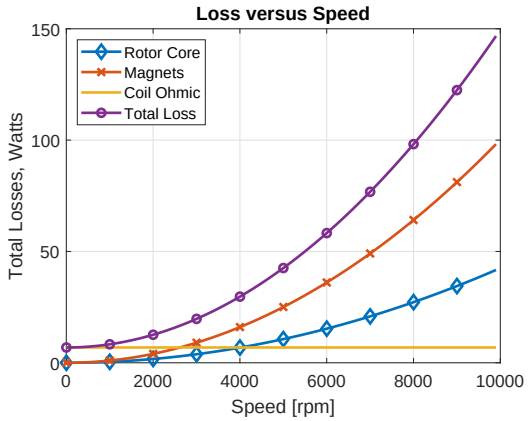

Fig. 6. Variable speed losses with high ripple current source

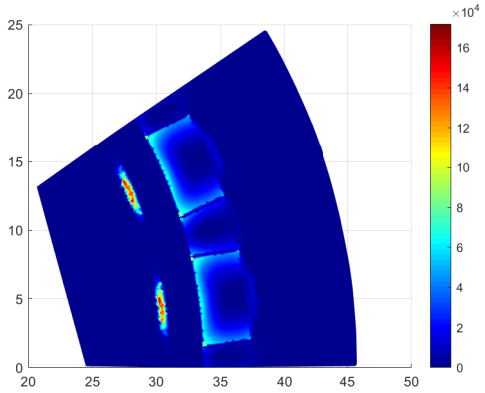

Fig. 8. Loss density (W/m^3) plot

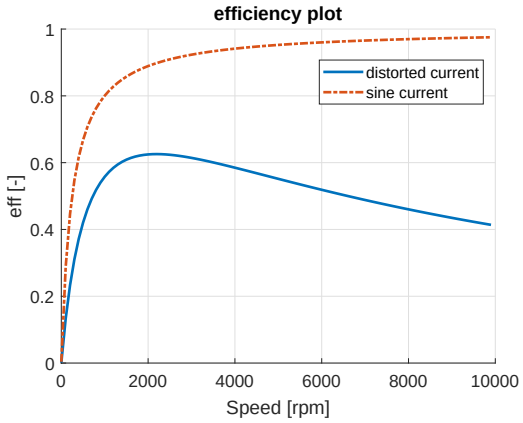

Fig. 7. Efficiency comparison with sinusoidal and distorted current source

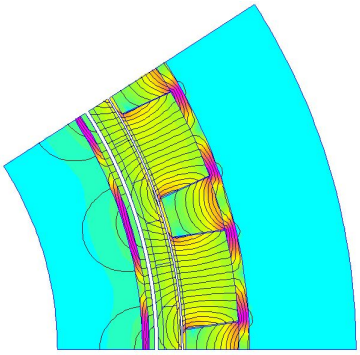

Fig. 9. Flux density plot

and without additional inductors is shown in Fig. 7.

Finally the loss density for the variable speed losses is shown in Fig. 8 the two spots in the inner rotating back/iron, with the highest loss density value, are located in the only part of the iron which is nominally non/saturated by the main flux as Fig. 9 shows. This means that the variable flux in the back iron induced by the harmonics, is not enough to move the operating point of the iron in those regions which are nominally saturated because of the magnets flux; whereas, in those non-saturated regions, the harmonic fields lead to a non negligible flux density variation that generates those "hot-spots".

VI. Experimental Results

The testing setup is shown in Fig. 10. The oscilloscope (DPO 4054B), along with a suitable current probe (P6021) are used to visualize the current waveform. A power analyser (WT1800) is used for measuring the input power to the motor. Even though only two currents and two line-to line voltages are needed for this purpose, the third current is still sent to a third channel in the power analyser, in order to balance out the three phases, and to use its signal in the power analyser as a reference for all the internal measurement, after being conveniently filtered by means of the embedded filtering features. This approach is needed for the power measurement without additional inductors, because the power analyser cannot synchronise the input signal, since it would require a stable signal with a well defined period, in order to measure power and harmonic content.

The test-rig was not mounting a torque sensor, and therefore, the torque constant, along with the fundamental current from the power analyser, were used to estimate the torque.

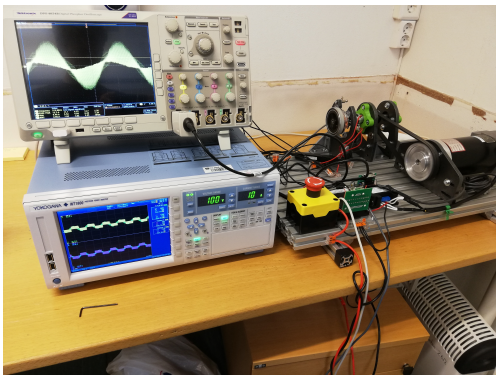

Fig. 10. Test-bench setup

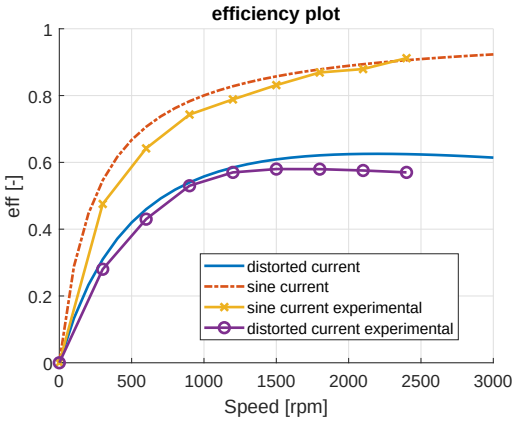

Fig. 11. Experimental efficiency results

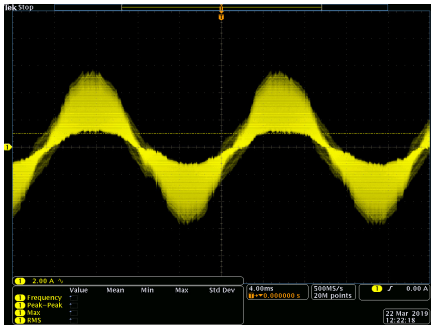

Fig. 12. Current from the oscilloscope 300 rpm 0.1 Nm

In the testing phase a brushed DC motor is controlled in speed mode as a brake, while the tested prototype is controlled in torque mode; under this setting all the mechanical losses are in charge of the brake motor. The torque was kept constant as the fundamental current was measured by means of the power analyser, and the efficiency was measured with steps of 300 rpm up to 2400 rpm. In Fig. 11 the experimental results are shown, along with the model results in the same range for a comparison.

In order to prove the drive model results Fig. 12 was taken from the oscilloscope once the same references which led to the current waveform in Fig. 3 were set in the bench (reference speed at the brake: 300[rpm]; torque reference at the motor: 0.1[Nm])

VII. Conclusion

Given the many starting assumptions for setting up the loss analysis method (especially if compared to the prototype used in this case study e.g. non laminated back-iron), and having neglected terms of additional losses which might be relevant (e.g. proximity losses in the windings, additional losses due to the many connections in the test-setup), the method cannot be defined accurate as such. This leaves some space for future improvements of the method itself which, at least, shows a coherent trend of the efficiency if compared to the experimental one. Moreover, the framework, is meant to be as general as possible, in fact, one could change the switching algorithm at the power inverter (taking care that the remaining drive model is coherent with the latter one) and using another type of machine model

Acknowledgment

This project was performed in cooperation with Alva Motor Solutions which provided both the motor prototype and the test-rig; the authors are grateful to the whole group for the support. The authors would also like to thank the NTNU Department of Electric Power Engineering for having provided the measurement equipment during the testing phase.

References

[1] Aslan, B., Semail, E. and Legranger, J. (2014). General Analytical Model of Magnet Average Eddy-Current Volume Losses for Comparison of Multiphase PM Machines With Concentrated Winding. IEEE Transactions on Energy Conversion, 29(1), pp.72-83.

[2] G. Gotovac, G. Lampic, D. Miljavec, " Eddy currents in permanent magnets of a multi-pole direct drive motor. Acta Technica Jaurinensis," 2013, 6(1), 133-140.

[3] Sakai, K. and Washizu, T. (1993). Structure and Characteristics of a High Speed Axial Gap Motor with Two Rotor Discs. IEEJ Transactions on Industry Applications, 113(8), pp.970-978.

[4] Y. Ma, L. Fan, and Z. Miao, "Realizing space vector modulation in MATLAB/Simulink and PSCAD," in North American Power Symposium (NAPS), 2013, 2013, pp. 1-6.

[5] Sarigiannidis, A. and Kladas, A. (2015). Switching Frequency Impact on Permanent Magnet Motors Drive System for Electric Actuation Applications. IEEE Transactions on Magnetics, 51(3), pp.1-4.

[6] A. S. Holter, "Design and Analysis of Stationary Reference Frame Controllers for Active Front End Converter," M. S. thesis, NTNU, Trondheim, NO, 2016.

[7] Saini, D., Ayachit, A., Reatti, A. and Kazimierczuk, M. (2018). Analysis and Design of Choke Inductors for Switched-Mode Power Inverters. IEEE Transactions on Industrial Electronics, 65(3), pp.2234-2244.

[8] Nan, X. and Sullivan, C. (2009). An Equivalent Complex Permeability Model for Litz-Wire Windings. IEEE Transactions on Industry Applications, 45(2), pp.854-860.

[9] Doc.ingeniamc.com. (2019). Everest XCR - Product Manual - Everest XCR. [online] Available at: http://doc.ingeniamc.com/everest-xcr/manuals/everest-xcr-product-manual [Accessed 31 Mar. 2019].

[10] Femm.info. (2019). Finite Element Method Magnetics: Rotating Losses in a Surface Mount Permanent Magnet Motor. [online] Available at: http://www.femm.info/wiki/SPMLoss [Accessed 31 Mar. 2019].

[11] Femm.info. (2019). Finite Element Method Magnetics: Sliding band motion model for electric machines. [online] Available at: http://www.femm.info/wiki/SlidingBand [Accessed 31 Mar. 2019].

[12] T. Nakata, Y. Ishihara and M. Nakano, Memoirs of the School of Engineering, Okayama University, Vol. 8,NO. 1, pp 1-14, 1973.

[13] Lavers, J., Biringer, P. and Hollitscher, H. (1978). A simple method of estimating the minor loop hysteresis loss in thin laminations. IEEE Transactions on Magnetics, 14(5), pp.386-388.